JCTC Journal of Chemical Theory and Computation

pubs.acs.org/JCTC Article

Accurate Full-Dimensional Global Diabatic Potential Energy Matrix for the Two Lowest-Lying Electronic States of the H + O_2 ↔ HO + O Reaction

Junyan Wang,[#] Feng An,[#] Junjie Chen, Xixi Hu,* Hua Guo,* and Daiqian Xie*

Cite This: *J. Chem. Theory Comput.* 2023, 19, 2929−2938 Read Online

ACCESS | Metrics & More | Article Recommendations | Supporting Information

ABSTRACT: A new and more accurate diabatic potential energy matrix (DPEM) is developed for the two lowest-lying electronic states of HO_2, covering both the strong interaction region and reaction asymptotes. The *ab initio* calculations were performed at the Davidson corrected multireference configuration interaction level with the augmented correlation-consistent polarized valence quintuple-zeta basis set (MRCI +Q/AV5Z). The accuracy of the electronic structure calculations is validated by excellent agreement with the experimental HO_2 equilibrium geometry, fundamental vibrational frequencies, and H + O_2 ↔ OH + O reaction energy. Through the combination of an electronic angular momentum-method and a configuration interaction vector-based method, the mixing angle between the first two $^2A''$ states of HO_2 was successfully determined. Elements of the 2×2 DPEM were fit to neural networks with a proper account of the complete nuclear permutation inversion symmetry of HO_2. The DPEM correctly predicted the properties of conical intersection seams at linear and T-shape geometries, thus providing a reliable platform for studying both the spectroscopy of HO_2 and the nonadiabatic dynamics for the H + O_2 ↔ OH + O reaction.

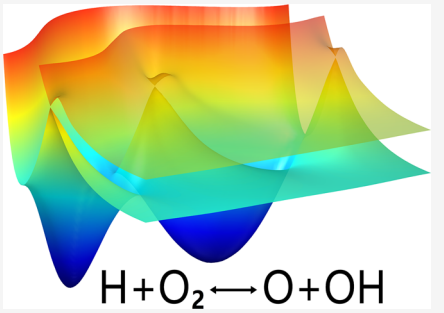

1. INTRODUCTION

As a key transient species, the hydroperoxyl radical (HO_2) plays an important role in combustion, where the rate-limiting chain-branching H + O_2 → HO_2 → OH + O reaction is considered as "the most important elementary step" in hydrocarbon combustion.[1] As a result, the HO_2 intermediate is a spectroscopically based target for flame diagnostics. This reaction and its reverse are also involved in a variety of atmospheric processes,[2] such as nighttime ozone destruction via the reverse reaction. The barrierless OH + O reaction is believed to be relevant in astrochemistry as well.[3] Given its importance in gas phase chemistry, the spectrum and kinetics/dynamics of this species have been the subject of extensive studies in the past.[4−12]

In the adiabatic approximation, the nuclear dynamics of a molecular system relies on the corresponding Born−Oppenheimer potential energy surface (PES), which is the dependence of electronic (and nuclear repulsion) energy on molecular geometry. There have been several versions of the global reactive PES based on *ab initio* calculations for the ground electronic state $HO_2(\tilde{X}^2A'')$,[13−20] as well as an excited state $HO_2(\tilde{A}^2A')$.[21] The ground state PES developed more than 15 years ago by Xu, Xie, Zhang, Lin, and Guo (XXZLG)[18] has been extensively used to understand the HO_2 spectrum and the H + O_2 ↔ O + OH reaction dynamics and kinetics.[22−35]

Although the adiabatic approach has been quite successful in describing the nuclear dynamics of this system, it is long known that this is an approximation because of the presence of low-lying excited states that intersect with the ground electronic state.[17,36] The two lowest-lying A'' electronic states are coupled by a common type of electronic degeneracy called conical intersections (CIs),[37,38] which break down the single-state Born−Oppenheimer approximation. For these two states of HO_2, there are three CIs located at the $C_{\infty v}$ (two equivalent ones due to the permutation symmetry of the two O nuclei in the molecule) and C_{2v} geometries near the H+O_2 asymptote,[17] as illustrated in Figure 1. In fact, these CIs are one-dimensional seams that are required by symmetry. Very recently, it was shown that the T-shape CI plays an important role in the H +O_2 scattering and the O + OH → H + O_2 reaction at ultracold conditions even when the energy is substantially below the lowest crossing point of the CIs.[39−41] This is because the presence of a CI introduces a vector potential in the adiabatic Hamiltonian due to the so-called geometric phase (GP),[42,43] which changes the sign of the electronic wave

Received: March 13, 2023
Published: May 10, 2023

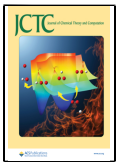

https://doi.org/10.1021/acs.jctc.3c00291
J. Chem. Theory Comput. 2023, 19, 2929−2938

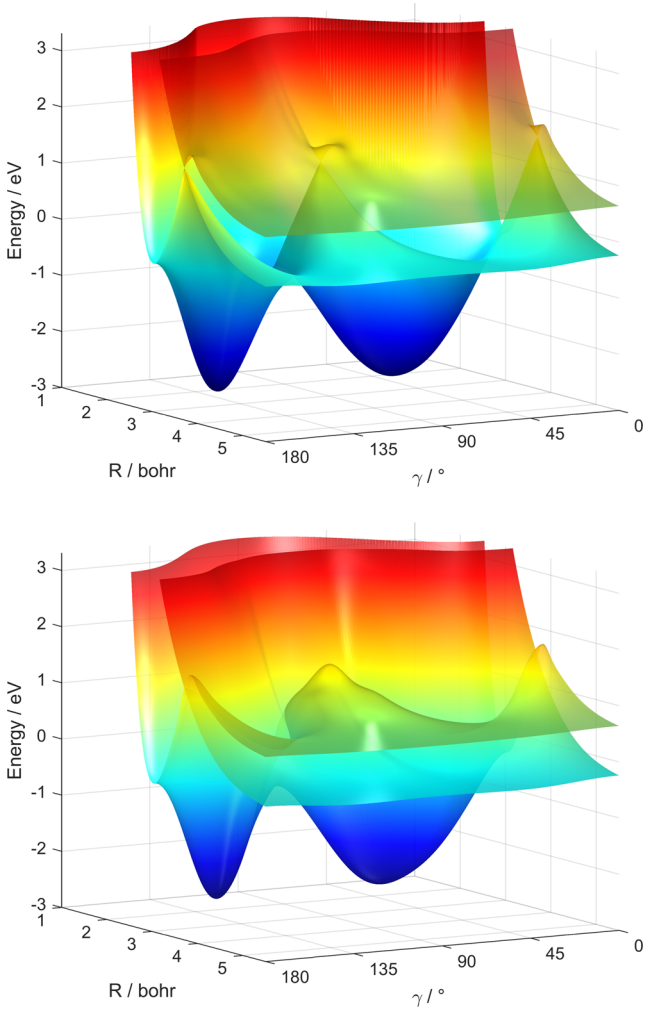

Figure 1. Adiabatic (upper panel) and diagonal diabatic (lower panel) PESs for the two lowest-lying electronic states of HO_2 as a function of the H−O_2 Jacobi coordinates (R, γ) at r_{OO} = 2.45 bohr. The T-shape and linear CIs are clearly seen in the upper panel.

function as the system encircles the CI seam.[44−48] The vector potential results in numerical instability in the adiabatic treatment of the dynamics because the derivative coupling (and the diagonal Born−Oppenheimer correction) are singular at the CI seam.[49,50]

To study the impact of CIs on nuclear dynamics, it is more convenient to work within a diabatic representation, in which the singularity in the adiabatic kinetic energy operator is removed and the potential energy operator can be accurately represented by an analytical diabatic potential energy matrix (DPEM).[45,51] The construction of a globally accurate DPEM is challenging, but once available it allows robust and accurate characterization of the dynamics.[52] The recent studies on the nonadiabatic dynamics in the title reaction have used a DIM (diatom-in-molecule) form for the DPEM, with parameters determined by *ab initio* calculations.[17] While the DIM DPEM correctly predicts the three CIs, the inflexible DIM form makes it hard to be quantitatively accurate in the entire relevant configuration space. In addition, the level of theory used to generate the *ab initio* points can now be significantly improved with increased computational power.

In this work, we report a high accuracy global reactive DPEM for the hydroperoxyl radical, covering the entire reaction path for the title reaction. The *ab initio* calculations were carried out using a multireference method with a large basis set. Taking advantage of diabatization schemes based on both properties and configuration interaction vectors (CIVs), the diabatic potentials and their coupling were determined for the two lowest-lying A'' electronic states of HO_2 in the entire relevant configuration space. The new DPEM is represented with high fidelity by a neural network (NN) method, which gives excellent agreement with the measured equilibrium geometry, fundamental frequencies, and reaction energy on the ground electronic state PES of $HO_2(\tilde{X}^2A'')$. It is thus expected to provide an accurate platform for both adiabatic and nonadiabatic studies of the corresponding nuclear dynamics. This work is organized as follows. The details of *ab initio* calculations, diabatization, and fitting are presented in Sec. 2. The results of DPEM and its properties are discussed in Sec. 3. Conclusions are given in Sec. 4.

2. THEORY

2.1. *Ab Initio* Calculations. For the HO_2 molecular system, 9 active orbitals ($7a' + 2a''$ in C_s symmetry, corresponding to $4a_1 + 1b_1 + 3b_2 + 1a_2$ in C_{2v} symmetry) and 13 electrons were included in the active space. *Ab initio* calculations of the two electronic states of HO_2 (two lowest-lying $^2A''$ electronic states in C_s symmetry) were performed by using the internally contracted multireference configuration interaction[53,54] augmented with the Davidson correction with a rotated reference,[55] denoted as icMRCI+Q_{rot}. The augmented correlation-consistent polarized valence quintuple-zeta (AV5Z) basis set[56] was used for oxygen and hydrogen. Extensive convergence tests have been performed and the results are shown in Table S1 in the Supporting Information (SI). In order to smoothly represent the character for those states, a six-state averaged (three A' and three A'') completed active space self-consistent field (SA-CASSCF) wave functions[57,58] were calculated and used in the MRCI calculations. All *ab initio* calculations were carried out in C_s symmetry using the MOLPRO 2015.1 package.[59]

2.2. Diabatization. While the *ab initio* calculations are performed in the Born−Oppenheimer adiabatic representation, it is advantageous to work in a diabatic representation for a number of reasons.[45,46,52] Most importantly, diabatization removes singular operators such as the derivative coupling, making the dynamical calculations numerically stable. It also allows an analytical representation of the diabatic PESs and their couplings, which are smooth functions of nuclear coordinates. The two representations are related by the (nuclear coordinate dependent) adiabatic-to-diabatic (AtD) unitary transformation, but its determination is not straightforward. In addition, diabatization for polyatomic systems is not unique because the derivative coupling cannot be removed completely unless all electronic states are included in the consideration.[60,61]

There exist several different strategies for diabatization.[51,62] Even though the derivative coupling based methods are the most reliable,[52] the computational cost for calculating the derivative coupling is rather high. In this work, we use a mixed diabatization strategy that takes advantage of the fact that electronic properties follow smoothly with the diabatic bases and can thus serve as a reporter of the electronic degeneracy (e.g., CIs) and that configuration interaction coefficients make abrupt changes at the CI seam due to change of electronic character. In particular, various properties can be used to treat

https://doi.org/10.1021/acs.jctc.3c00291
J. Chem. Theory Comput. 2023, 19, 2929−2938

different types of CIs. For the linear CI, it is convenient to use the diabatization strategy of Dobbyn and Knowles,[63] improved by van Harrevelt and van Hemert for AB_2 systems,[64] which employs the electronic orbital angular momentum in determining the mixing angle between the two electronic states. This approach has been successfully demonstrated in constructing a DPEM for the H_2O system, where two $\tilde{B}-\tilde{X}$ CIs exist in linear geometries.[63−65] While T-shape CIs, the CIV method[66] is more suitable for determining the mixing angle, which has been successfully adapted to construct a DPEM for several systems, such as H_2S,[66] NO_2,[67] and SO_2.[68] Since the HO_2 system contains both linear and T-shape CIs, we used both strategies to obtain the AtD mixing angle and connected them to get the final result.

The two lowest-lying $^2A''$ states, as illustrated in Figure 1, are correlated with the $H(^2S)+O_2(X^3\Sigma_g^-)/O_2(a^1\Delta_g)$ and $O(^3P)+OH(X^2\Pi)$ asymptotes, respectively. The CIs in the HO_2 system are symmetry allowed.[69] While the $1^2A''$ and $2^2A''$ states have the same symmetry in C_s symmetry and their potentials thus cannot cross, they become $^2\Pi$ and $^2\Sigma^-$ states at collinear geometries, respectively, corresponding to the electronic angular momentum of $\Lambda = 1$ and 0, respectively. In linearity, the two states thus belong to different symmetries so they can cross in $C_{\infty v}$ symmetry. For the Π state, the degeneracy is lifted when the molecule bends, leading to a $^2A''$ and a $^2A'$ states. The $^2A''$ component forms the linear CI with another $^2A''$ state. In the C_{2v} symmetry, however, the two lowest-lying electronic states belong to the $^2A_2$ and $^2B_1$ symmetry species, respectively, which can also cross by the same principle and are thus responsible for another CI.

We restrict our effort in this work to the two lowest A'' states coupled by the CIs. The two diabatic states ($|\psi_i^{(d)}\rangle$) can be obtained from the two adiabatic states ($|\psi_i^{(a)}\rangle$) by a unitary AtD transformation:

$$\begin{pmatrix} |\psi_1^{(d)}\rangle \\ |\psi_2^{(d)}\rangle \end{pmatrix} = U \begin{pmatrix} |\psi_1^{(a)}\rangle \\ |\psi_2^{(a)}\rangle \end{pmatrix} \tag{1a}$$

with the AtD matrix defined by a mixing angle α, which depends on nuclear coordinates

$$U = \begin{pmatrix} \cos\alpha & \sin\alpha \\ -\sin\alpha & \cos\alpha \end{pmatrix} \tag{1b}$$

Here, the adiabatic states in eq 1a are identical to the $1^2A''$ and $2^2A''$ states.

For the angular momentum-based method used near the collinear geometry, the mixing angle α^{LZ} is extracted from electronic orbital angular momentum matrix elements as follows:[63,64]

$$\begin{aligned} \alpha^{LZ} &= \arcsin|L| \\ &= \arcsin\sqrt{|\langle 1^2A'|\hat{L}_z|1^2A''\rangle|^2 + |\langle 1^2A'|\hat{L}_y|1^2A''\rangle|^2} \end{aligned} \tag{2}$$

where $\hat{L}_z$ and $\hat{L}_y$ are the z and y components of the electronic angular momentum operator $\hat{L}$. Here, the molecule was fixed in the yz plane and the z axis was kept bisecting the OHO angle in all geometries. The $1^2A'$ state serves as a reference as it is not involved in the CIs. The above equation is in a symmetrized form with respect to the exchange of the two O nuclei, proposed by van Harrevelt and van Hemert.[64] Because the components of angular momentum $\hat{L}_z$ and $\hat{L}_y$ are not well-defined when molecule is far from linear geometry, such method cannot be used to describe the T-shape CI, as discussed in the SI.

For the CI at the C_{2v} geometry, we use the CIV method[66] to calculate the mixing angle near the C_{2v} geometry, which is implemented in MOLPRO.[59] This diabatization in $H+O_2$ Jacobi coordinates (R, r_{OO}, γ) requires two steps: first, the active orbitals of a CASSCF calculation are rotated to maximize the overlap with the orbitals at a C_{2v} reference geometry, of which the R and r_{OO} remain the same and the Jacobi angle γ is set to 90 deg. Second, nonadiabatic coupling matrix elements and mixing angle α^{CIV} can be computed by finite differences for MRCI wave functions using the DDR program in MOLPRO.

We modify the mixing angle with damping functions to get a dynamically convenient description in the asymptotic regions. Details of the implementation are given in the SI. To obtain the smoothly varying mixing angle, we connect the mixing angle obtained using different methods by a switch function as follows:

$$\alpha^{\text{final}} = \alpha_{\text{mod2}}^{LZ}(1-f) + \alpha_{\text{mod2}}^{CIV} f \tag{3}$$

in which $f = \frac{1}{1+e^{-\lambda(\gamma-\gamma_1)}}$, where $\lambda = 0.3$ deg^{-1}, and $\gamma_1 = 67$ deg. The $\alpha_{\text{mod2}}^{LZ}$ and $\alpha_{\text{mod2}}^{CIV}$ are modified mixing angle from angular momentum and CIV based method. α^{final} is the final mixing angle used on each point. This function will not change the mixing angle near the two type CIs, only make a smooth connection in the region away from the intersections.

The DPEM can finally be expressed as a unitary transformation of the adiabatic potential energy matrix, which is diagonal with the adiabatic energies E_1 and E_2, as follows:

$$V^d = UV^aU^T \tag{4}$$

in which the AtD matrix is defined with the modified mixing angle and ^{T} denotes the transpose.

To examine properties the CIs, we follow a closed loop around the CI seam in its vicinity. By moving the H atom, a small and enclosed circle can be defined to probe the derivative coupling $\tau_{12}(\varphi|\rho)$ around a CI, defined by a small radius (ρ) and a polar angle (φ). Within the two-state model, the derivative coupling $\tau_{12}(\varphi|\rho)$ is defined as follows:[70,71]

$$\tau_{12}(\varphi|\rho) = \left\langle \psi_1^a(\varphi|\rho) \middle| \frac{\partial}{\partial\varphi} \middle| \psi_2^a(\varphi|\rho) \right\rangle \tag{5}$$

The mixing angle $\alpha_{12}(\varphi|\rho)$ can then be obtained from the derivative coupling:[61]

$$\alpha_{12}(\varphi|\rho) = \int_0^{\varphi} \tau_{12}(\varphi'|\rho)\mathrm{d}\varphi' \tag{6}$$

Along the closed loop around CIs, this integral in eq 6 should yield π as follows:[45]

$$\alpha_{12}(\rho) = \int_0^{2\pi} \tau_{12}(\varphi'|\rho)\mathrm{d}\varphi' = \pi \tag{7}$$

which is the origin of the geometric phase.

From the DPEM, the derivative coupling can be readily obtained from the elements V_{11}, V_{22}, and V_{12}:[72]

https://doi.org/10.1021/acs.jctc.3c00291
J. Chem. Theory Comput. 2023, 19, 2929−2938

$$\tau_{12}(\varphi|\rho) = \frac{\partial\alpha}{\partial\varphi} = \frac{\left[\frac{\partial V_{12}}{\partial\varphi}(V_{11} - V_{22}) - V_{12}\left(\frac{\partial V_{11}}{\partial\varphi} - \frac{\partial V_{22}}{\partial\varphi}\right)\right]}{\left[1 + \left(\frac{2V_{12}}{V_{11} - V_{22}}\right)^2\right](V_{11} - V_{22})^2} \tag{8}$$

2.3. Fitting and Permutation Symmetry. To provide an analytical representation of the DPEM, the diabatic permutation invariant polynomial-neural network (PIP-NN) method[72] was used. The idea of PIP-NN is to used PIPs[73] as the input layer of a NN, which enforces the permutation symmetry of the system.[74,75] This approach has been successfully applied to many systems,[76−81] thanks to the ultraflexibility of the NN and the ability to enforce permutation symmetry.[82,83] In the system discussed here, the two diagonal and one off-diagonal elements are represented by three NNs.

The complete nuclear permutation and inversion (CNPI) group[84] for HO_2 is isomorphic to the C_{2v} point group, for which the character table is given in Table 1. To illustrate the CNPI symmetry, we choose a point at the C_{2v} symmetry, where the two diabatic states belong to the A_2 and B_1 irreducible representations. Since the diabatic states by definition maintain the CNPI symmetries in other geometries throughout the configuration space, these two symmetry species can thus be used to discuss the CNPI symmetry of the system. While the diagonal elements of the DPEM (V_{11} and V_{22}) belong to the totally symmetric irreducible representation ($A_2 \times A_2 = B_1 \times B_1 = A_1$), the off-diagonal element V_{12} belongs to the B_2 ($A_2 \times B_1 = B_2$) irreducible representation that is antisymmetric with respect to the exchange of the two oxygen nuclei.

Table 1. Character Table of the CNPI Group of HO_2 and the Isomorphic C_{2v} Point Group

CNPI	E	(12)	(12)*	E^*
C_{2v}	E	C_2	σ_h	σ_v
A_1	1	1	1	1
A_2	1	1	−1	−1
B_1	1	−1	1	−1
B_2	1	−1	−1	1

The following three PIPs were used as the input layer of the three NNs:

$$G_1 = \frac{p_{13} + p_{23}}{2}, \quad G_2 = p_{13}p_{23}, \quad G_3 = p_{12} \tag{9}$$

where the O, O, and H atoms are labeled as 1, 2, and 3, respectively. The PIPs are symmetrized monomials of Morse-like variables:[73]

$$p_{ij} = e^{-r_{ij}/a} \tag{10}$$

where r_{ij} represents the internuclear distance between the ith and jth atoms and a is the parameter to describe the decay rate of the monomial with the internuclear distance (a = 2 bohr is used in this work). To satisfy the permutation antisymmetry for the off-diagonal element V_{12} and keep it exactly equal to zero in both linear or C_{2v} geometries, the $V_{12}/\sin(2\gamma)$ is fitted using the PIP-NN method, where γ is the Jacobi angle.

NNs with two hidden layers of 20 and 20 neurons were trained with the Levenberg−Marquardt algorithm, where the root-mean-square errors (RMSEs) were used to evaluate the fitting performance:

$$\mathrm{RMSE} = \sqrt{\sum_{i=1}^{N} w_i(E_{\mathrm{fitting}} - E_{ab\ initio})^2 / \sum_{i=1}^{N} w_i} \tag{11}$$

where $E_{ab\ initio}$ and E_{fitting} are the input energies and the fitted ones, respectively, and N is the number of *ab initio* points. In order to fit the important regions more accurately, we increase the weights w_i for the geometries around the equilibrium geometry, CIs, and the asymptote regions. The *ab initio* points are randomly divided into training (90%), validation (5%), and testing sets (5%), respectively. The training set was used in the NN training, while the validating set was used in the early stopping scheme[85] to avoid overfitting. The testing set was used to assess the fitting quality. The DPEM is available upon request from the corresponding author (D.X.).

3. RESULTS AND DISCUSSION

About 17 000 points were calculated and used to fit the 2×2 DPEM, using the PIP-NN method described above. These points extend to 25 bohr in both asymptotes. The RMSEs with equal weight factor for points below 3.0 eV (relative to the $O(^3P)+OH(X^2\Pi)$ asymptote) of the two diagonal elements of the DPEM are 11.9 and 8.8 meV, while that for the off-diagonal term is 9.9 meV. In Table 2, the equilibrium geometry of $HO_2(\tilde{X}^2A'')$, fundamental vibrational frequencies, and dissociation energies on the PES are compared with previous theoretical and available experimental results. The calculated equilibrium geometry is in excellent agreement with the experiment.[86] The calculated dissociation energies D_e(H−OO) and D_e(O−OH) are found to be 2.367 and 2.930 eV, which

Table 2. Comparison of Theoretical and Experimental Results for the Equilibrium Geometry (r_{OH}/bohr, r_{OO}/bohr, θ_{OOH}/deg), Dissociation Energies (in eV) and Vibrational Energy Levels (in cm^{-1}) of the Ground State of the HO_2 Radical as well as the Diatoms

				Vibrational frequencies					
				HO_2 (ν_1, ν_2, ν_3)			OH/O_2		
HO_2	(r_{OH}, r_{OO}, θ_{OOH})	D_e(H−OO)	D_e(O−OH)	(0, 0, 1)	(0, 1, 0)	(1, 0, 0)	$O_2(^3\Sigma_g^-)$	$O_2(^1\Delta_g)$	$OH(^2\Pi)$
This work	(1.837, 2.507, 104.1)	2.367	2.930	1108.4	1384.9	3429.2	1549	1477	3570
XXZLG[a]	(1.836, 2.521, 104.1)	2.324	2.864	1090.7	1389.0	3430.0	/	/	/
DMBE IV[b]	(1.835, 2.514, 104.3)	2.379	2.961	1065.5	1296.4	3333.7	/	/	/
DIM[c]	(1.84, 2.52, 100.6)	2.246	2.828	/	/	/	/	/	/
Expt.	(1.834, 2.514, 104.3)[d]	2.369[e]	2.969[e]	1097.6[g]	1391.8[g]	3436.2[h]	1556[i]	1484[i]	3570[i]
		2.334[f]	2.934[f]						

[a]Ref 18. [b]Ref 16. [c]Ref 17. [d]Ref 86. [e]Ref 87. [f]Ref 88. [g]Ref 10. [h]Ref 5. [i]Ref 90.

https://doi.org/10.1021/acs.jctc.3c00291
J. Chem. Theory Comput. 2023, 19, 2929−2938

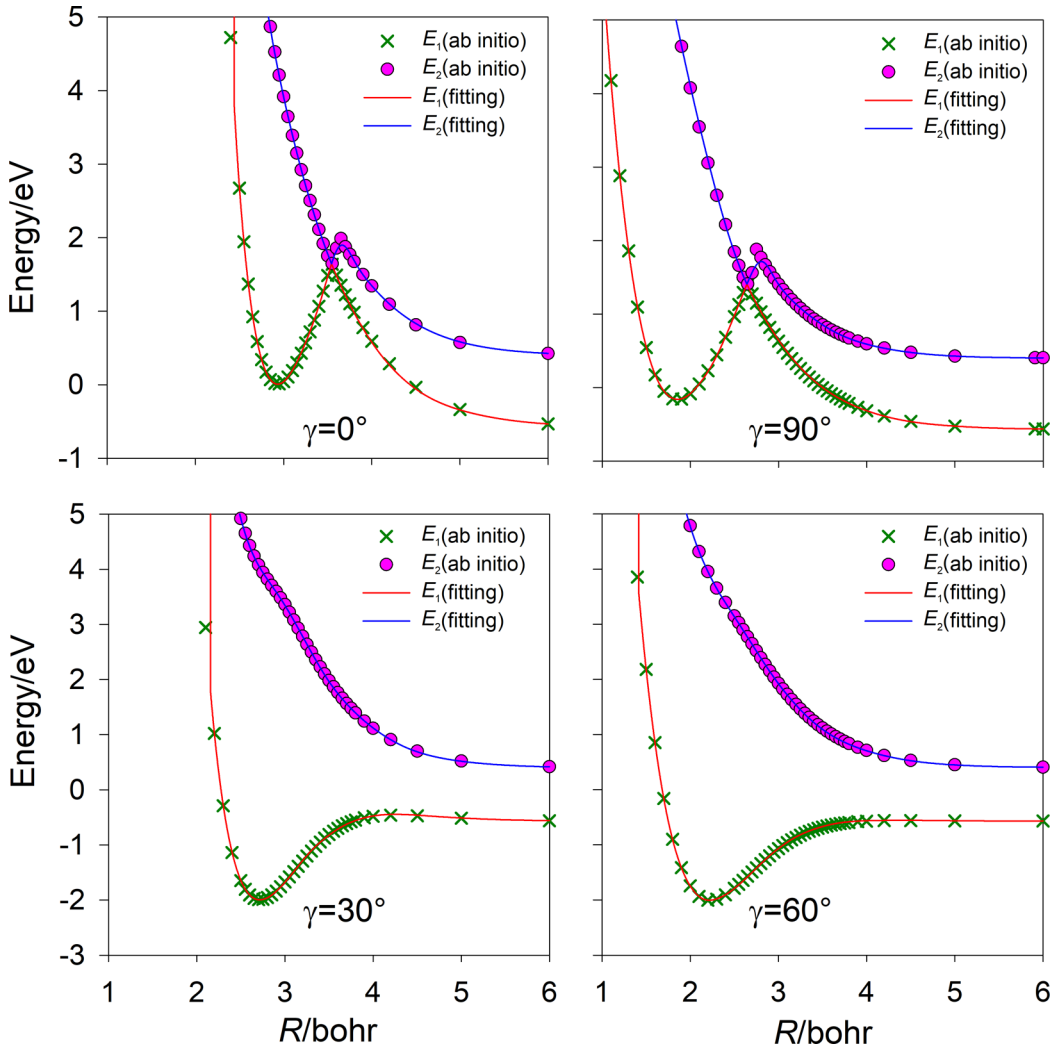

Figure 2. Comparison between *ab initio* (symbols) and DPEM (solid lines) adiabatic energies along the H−O_2 Jacobi coordinate R, with angle γ = 0, 30, 60, and 90 deg, and r_{OO} = 2.28 bohr.

are in good agreement with those computed from experimental measurements by $D_e = D_0 - ZPE_{H-OO/O-OH} + ZPE_{HOO}$.[87,88] At the same time, the ZPE-corrected endothermicity obtained from current PES is 0.696 eV, which is in better agreement with the recent experiment (0.718 eV)[88] than the previous XXZLG PES (0.659 eV).[18] In the same table, the calculated fundamental frequencies of $HO_2(\tilde{X}^2A'')$ are compared with available experimental band origins.[5,10] The vibrational levels are labeled by three vibrational quantum numbers v_1, v_2, and v_3, which represent the OH stretching, HOO bending, and O−O stretching modes, respectively. The calculated fundamental frequencies for these modes (v_1 is 3429.2 cm^{-1}, v_2 is 1384.9 cm^{-1}, and v_3 is 1108.4 cm^{-1}) are in quite good agreement with the experimental band origins (3436.2 cm^{-1}, 1391.8 cm^{-1}, and 1097.6 cm^{-1}). The OH and O_2 vibrational frequencies are also compared with the experimental values and the agreement is equally good.

In Figure 1, the PESs for the two adiabatic states from the new DPEM are displayed as a function of H−O_2 Jacobi coordinates R and γ, with r_{OO} fixed at 2.45 bohr. The two linear CIs and the T-shape one are clearly seen, whose cone shaped cusps are impossible to represent analytically. The corresponding diabatic PESs are shown in the same figure, and they are smooth functions of the nuclear coordinates and are thus much easier to obtain a high fidelity fit. To illustrate the high fidelity of the fitting, discrete *ab initio* energies are compared in Figure 2 with the adiabatic potentials obtained by diagonalizing the DPEM along the R coordinate at several different angles. It is clear that the fitting is highly faithful, particularly in the vicinity of the CI.

To examine the property of CI seams more closely, we calculated the derivative coupling and AtD mixing angle along a closed loop encircling each CI, and the results are shown in Figures 3 and 4. The coordinates for defining the loop in the vicinity of the CI are given in the figure. The polar angle φ along the circle is extended to $[0, 2\pi]$ to satisfy the requirement that the line integral of the derivative coupling τ along a closed loop around a CI yields a value of π.[45] Figure 3(a) shows diabatic potential energy curves (V_{11} and V_{22}) and adiabatic ones (E_1 and E_2 for the ground $1^2A''$ state and excited $2^2A''$ state) as a function of φ encircling the T-shape CI for the first two $^2A''$ state of HO_2. The circle around the T-shape CI is shown as the inset (R_{CI} = 2.7 bohr, r_{OO} = 2.28 bohr, ρ = 0.2 bohr) in Figure 3(b). Figure 3(b) shows V_{12} as a function of φ encircling the T-shape CI, and Figure 3(c) shows the corresponding derivative coupling τ_{12} and AtD mixing angle α_{12} as a function of φ encircling the CI. It can be readily seen that the derivative coupling τ_{12} is symmetric with respect to φ

https://doi.org/10.1021/acs.jctc.3c00291
J. Chem. Theory Comput. 2023, 19, 2929−2938

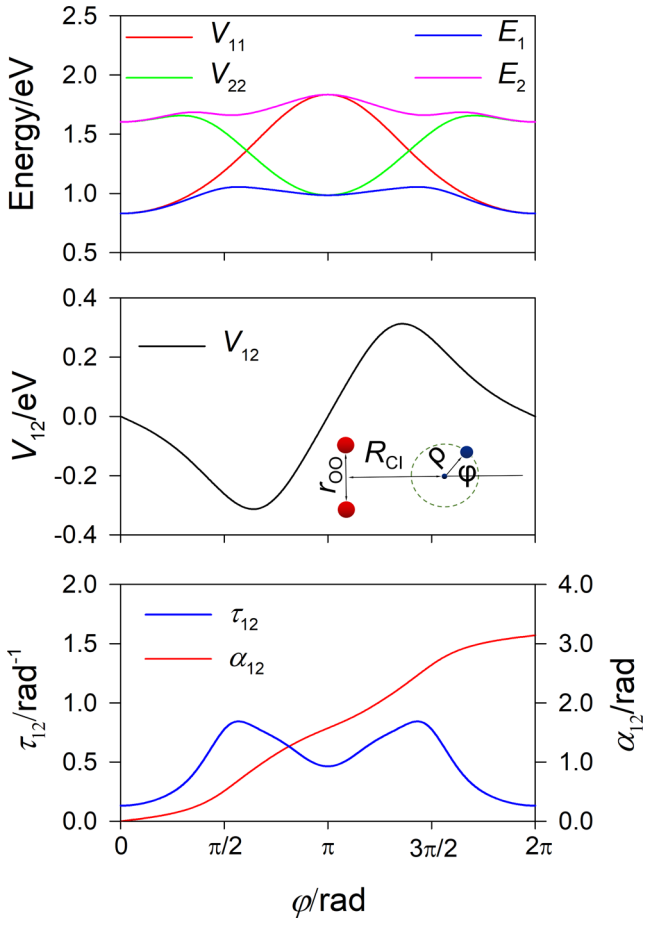

Figure 3. Adiabatic and diabatic potentials (upper panel), the diabatic coupling (middle panel), and the derivative coupling and the AtD mixing angle (lower panel) along a small circle around the T-shape CI. The radius and angle of the circle are defined in the inset with R_{CI} = 2.7 bohr, r_{OO} = 2.28 bohr, ρ = 0.2 bohr.

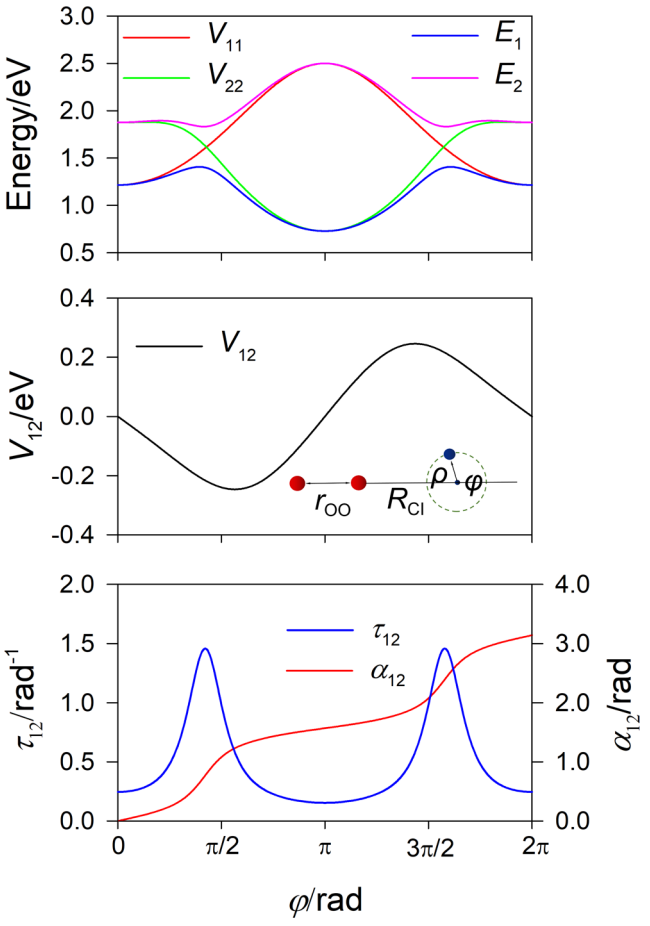

Figure 4. Adiabatic and diabatic potentials (upper panel), the diabatic coupling (middle panel), and the derivative coupling and the AtD mixing angle (lower panel) along a small circle around the linear CI. The radius and angle of the circle are defined in the inset with R_{CI} = 3.5 bohr, r_{OO} = 2.28 bohr, ρ = 0.2 bohr.

= π but the mixing angle α_{12} is antisymmetric, thanks to the antisymmetric character of V_{12}. As expected, the integral in eq 7 along the closed loop around the CI yields exactly the value π, reproducing the GP associated with the CI. The same geometric quantization is observed as well around the linear CIs (R_{CI} = 3.5 bohr, r_{OO} = 2.28 bohr, ρ = 0.2 bohr), which is shown in Figure 4.

The sign change of the V_{12} at the C_{2v} and $C_{\infty v}$ geometries is shown in a global perspective in Figure 5, where the O_2 is fixed at r_{OO} = 2.28 bohr. It is particularly worth noting the antisymmetry at the linear geometry, which is difficult to implement and often ignored.

In Figure 6, we compare the adiabatic potential curves of the current and the DIM[17] DPEMs in the Jacobi coordinate in the T-shape and linear configurations. The location and energy of the CIs for this work are consistent with the DIM values. In Table 3, the geometry and energy of the minimum energy crossing (MEX) of the two CIs are compared and there are significant quantitative differences. In addition, we note that the potential energy curves from the two DPEMs are not identical for either the ground or excited state. The difference on the $2^2A''$ state is quite large, due apparently to the different number of diabatic states included in these models.

In Figure 7, the adiabatic PES for the ground electronic state of HO_2 is plotted in the H−O and O−O bond distances at

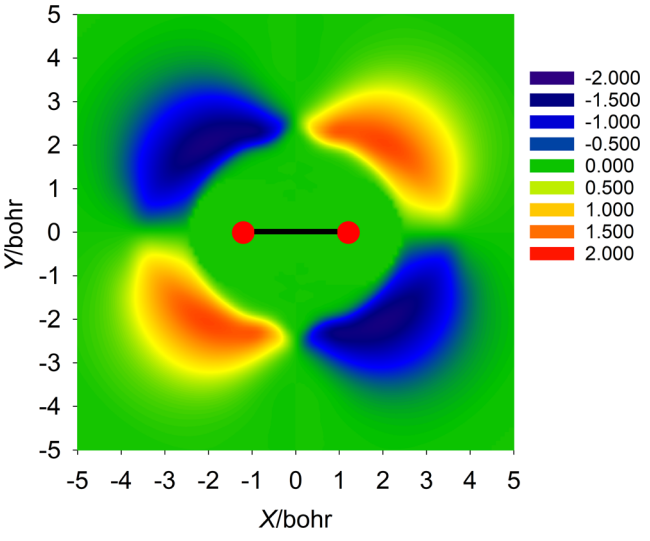

Figure 5. Contour plot of the off-diagonal element of the DPEM as a function of the H coordinates (X, Y) around O_2, which is fixed at r_{OO} = 2.28 bohr and placed at the origin along the X-axis in the X−Y plane.

several O−O−H bond angles θ. The HO_2 well is clearly seen in the figure. It is also apparent that the approaching of the H

https://doi.org/10.1021/acs.jctc.3c00291
J. Chem. Theory Comput. 2023, 19, 2929−2938

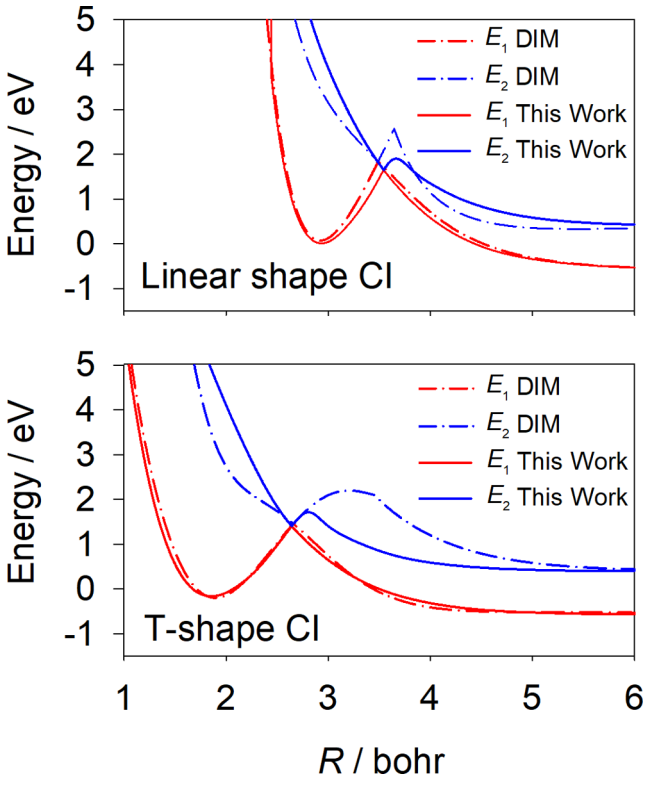

Figure 6. Comparison of the adiabatic potential energy curves along the R coordinate (with r_{OO} fixed at 2.28 bohr) from the current and DIM DPEMs in the T-shape and linear configurations.

Table 3. Comparison of Minimum Energy Crossing (MEX) Geometries (bohr and deg) and Energies (eV) Relative to the $O(^3P)+OH(X^2\Pi)$ Asymptote between the Current and DIM DPEMs

	T-shape MEX		linear MEX	
	(R, r_{OO}, γ)	Energy	(R, r_{OO}, γ)	Energy
this work	(2.82, 2.46, 90)	1.13	(3.67, 2.41, 0)	1.48
DIM[a]	(2.80, 2.43, 90)	1.32	(3.58, 2.38, 0)	1.75

[a]Ref 17.

to O_2 at a bent geometry is barrierless, but there is a barrier in the collinear approach due apparently to the linear CI.

In the collinear geometry, there is a submerged exit channel barrier in the minimum energy path leading to the OH+O asymptote. As discussed extensively in the literature,[16−18,89] the long-range minimum is formed in a collinear geometry due to the strong dipole−quadrupole interaction, as shown in Figure 8, where the ground state PES is plotted in the (r_{OO} and θ) coordinates with the O−H bond length optimized. Shown in the same figure, the submerged barrier at a nonlinear geometry separates this long-range well with the deep HO_2 well. On the current PES, the long-range minimum and the barrier are 645.3 and 482.0 cm^{-1} lower than the O+OH asymptote, respectively.

Finally, the $H+O_2$ channel is plotted in Figure 9 within the O−O bond length optimized. Unlike the O+OH channel, the interaction between H and O_2 is relatively weak. Due to the three CIs in the $H+O_2$ channel, local barriers exist around 0, $\pi/2$, and π. The minimum energy pathway is also performed in the same plot; there is no barrier in the $H+O_2$ entrance process leading to the global HO_2 well.

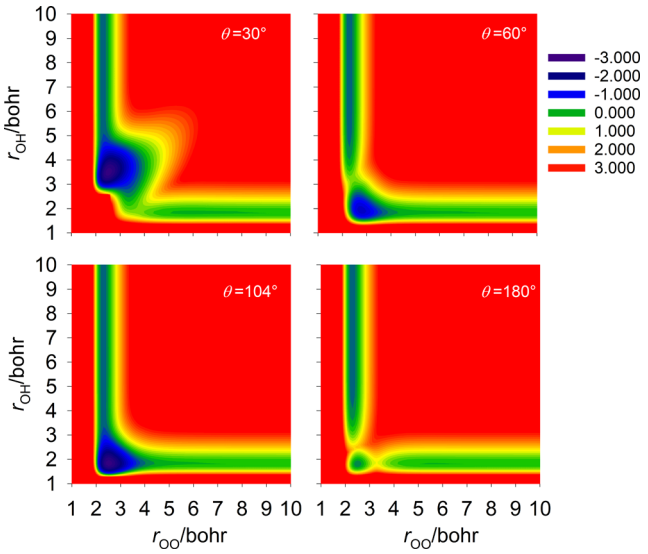

Figure 7. Contour plots of the ground state adiabatic PES in the O−O and O−H distances for different interbond angles. The θ = 180 deg corresponds to the collinear H−O−O geometry. The contours are given in eV relative to the $O(^3P)+OH(X^2\Pi)$ asymptote.

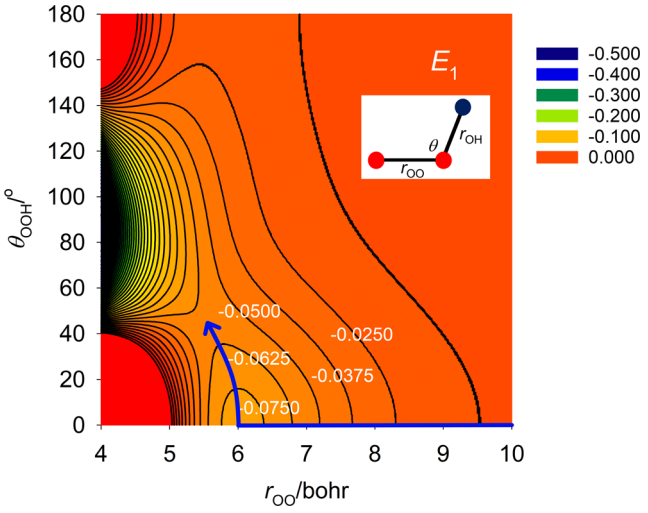

Figure 8. Contour plot of the ground state adiabatic PES in the O−O distance and interbond angle θ with the O−H distance optimized. The PES in the OH+O asymptote is dominated by a collinear well due to electrostatic interaction between OH and O, and a submerged barrier between this collinear minimum and the HO_2 chemical well, as shown by the minimum energy path in blue. The contours are given in eV relative to the $O(^3P)+OH(X^2\Pi)$ asymptote.

4. CONCLUSIONS

In this work, we report a new and more accurate DPEM for the two lowest-lying electronic states of HO_2, which are coupled by two equivalent linear CIs and one T-shape CI. The DPEM was constructed using the PIP-NN method, which has high fitting fidelity and preserves the correct permutation symmetry for the two identical O nuclei, from a large number of points at the MRCI+Q/AV5Z level of theory. The diabatization was carried out with a mixed method using both the electronic angular momentum and CIVs, which correctly follows the diabatic states. The new DPEM not only reproduces the structural, energetic, and spectroscopic properties of the ground state $HO_2(\tilde{X}^2A'')$, but it also correctly describes the

https://doi.org/10.1021/acs.jctc.3c00291
J. Chem. Theory Comput. 2023, 19, 2929−2938

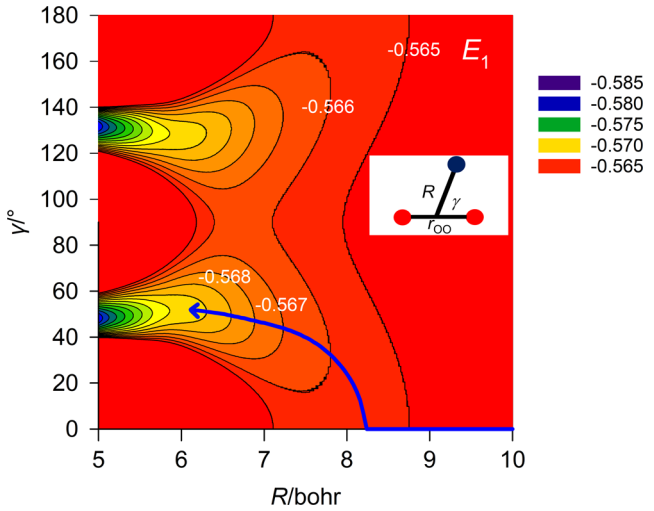

Figure 9. Contour plot of the adiabatic PES for the ground state in the H−O_2 Jacobi coordinates with the r_{OO} optimized. The energies are given in eV relative to the $O(^3P)$+$OH(X^2\Pi)$ asymptote.

three CIs between the two electronic states, including the GPs. It is expected to provide a reliable platform for investigating the spectroscopy of HO_2 and nonadiabatic dynamics for the H + O_2 ↔ OH + O reaction. We note in passing that the investigation of an ultracold reaction will require a more accurate representation of the long-range PES, which will be added in a future publication.

■ ASSOCIATED CONTENT

Supporting Information

The Supporting Information is available free of charge at https://pubs.acs.org/doi/10.1021/acs.jctc.3c00291.

The coverage tests of basis sets and discussion about angular momentum-based diabatization framework and detail of modification of the mixing angle (PDF)

■ AUTHOR INFORMATION

Corresponding Authors

Xixi Hu − *Kuang Yaming Honors School, Jiangsu Key Laboratory of Vehicle Emissions Control, Center of Modern Analysis, Nanjing University, Nanjing 210023, China; Hefei National Laboratory, Hefei 230088, China;* orcid.org/0000-0003-1530-3015; Email: xxhu@nju.edu.cn

Hua Guo − *Department of Chemistry and Chemical Biology, University of New Mexico, Albuquerque, New Mexico 87131, United States;* orcid.org/0000-0001-9901-053X; Email: hguo@unm.edu

Daiqian Xie − *Institute of Theoretical and Computational Chemistry, Key Laboratory of Mesoscopic Chemistry, School of Chemistry and Chemical Engineering, Nanjing University, Nanjing 210023, China; Hefei National Laboratory, Hefei 230088, China;* orcid.org/0000-0001-7185-7085; Email: dqxie@nju.edu.cn

Authors

Junyan Wang − *Institute of Theoretical and Computational Chemistry, Key Laboratory of Mesoscopic Chemistry, School of Chemistry and Chemical Engineering, Nanjing University, Nanjing 210023, China*

Feng An − *Research Center for Graph Computing, Zhejiang Lab, Hangzhou 311121, China*

Junjie Chen − *Institute of Theoretical and Computational Chemistry, Key Laboratory of Mesoscopic Chemistry, School of Chemistry and Chemical Engineering, Nanjing University, Nanjing 210023, China*

Complete contact information is available at: https://pubs.acs.org/10.1021/acs.jctc.3c00291

Author Contributions

#J.W. and F.A. have equal contributions.

Notes

The authors declare no competing financial interest.

■ ACKNOWLEDGMENTS

This work was supported by the Innovation Program for Quantum Science and Technology (2021ZD0303305 to D.X.), by the National Natural Science Foundation of China (Grant Nos. 22233003 and 22241302 to D.X., 22122302 and 22073042 to X.H.), and in part by Department of Energy (Grant No. DE-SC0015997 to H.G.). All calculations have been performed on the computing facilities in the High Performance Computing Center (HPCC) of Nanjing University. F.A. and J.W. thank Professor Changjian Xie and Professor Anyang Li for valuable advice about *ab initio* calculations. H.G. thanks Dr. Brian Kendrick for sharing with us the DIM DPEM.

■ REFERENCES

(1) Miller, J. A.; Kee, R. J.; Westbrook, C. K. Chemical-kinetics and combustion modeling. *Annu. Rev. Phys. Chem.* **1990**, *41*, 345−387.

(2) Warneck, P. *Chemistry of the Natural Atmosphere*; Academic Press: San Diego, 2000.

(3) Smith, I. W. M.; Herbst, E.; Chang, Q. Rapid neutral-neutral reactions at low temperatures: a new network and first results for TMC-1. *Mon. Not. R. Astron. Soc.* **2004**, *350*, 323−330.

(4) Howard, M. J.; Smith, I. W. M. Direct rate measurements on the reactions N+OH → NO+H and O+OH → O_2+H from 250 to 515 K. *J. Chem. Soc. Faraday Trans. 2* **1981**, *77*, 997−1008.

(5) Yamada, C.; Endo, Y.; Hirota, E. Difference frequency laser spectroscopy of the v_1 band of the HO_2 radical. *J. Chem. Phys.* **1983**, *78*, 4379−4384.

(6) Kleinermanns, K.; Linnebach, E. Experimental study of H + O_2 reaction dynamics at collision energies of 2.6, 1.9, and 1.0 eV. *J. Chem. Phys.* **1985**, *82*, 5012−5018.

(7) Bronikowski, M. J.; Zhang, R.; Rakestraw, D. J.; Zare, R. N. Reaction dynamics of H+O_2 at 1.6 eV collision energy. *Chem. Phys. Lett.* **1989**, *156*, 7−13.

(8) Jacobs, A.; Volpp, H. R.; Wolfrum, J. Absolute reactive cross sections for the reaction H + O_2 → OH + O. *Chem. Phys. Lett.* **1991**, *177*, 200−206.

(9) Kessler, K.; Kleinermanns, K. H + O_2 → OH + O: excitation functions and absolute reaction cross sections. *J. Chem. Phys.* **1992**, *97*, 374−377.

(10) Burkholder, J. B.; Hammer, P. D.; Howard, C. J.; Towle, J. P.; Brown, J. M. Fourier transform spectroscopy of the ν_2 and ν_3 bands of HO_2. *J. Mol. Spectrosc.* **1992**, *151*, 493−512.

(11) Kim, H. L.; Wickramaaratchi, M. A.; Zheng, X.; Hall, G. E. Reactions of velocity-aligned atoms probed by Doppler profiles: H +O_2 → OH+O. *J. Chem. Phys.* **1994**, *101*, 2033−2050.

(12) Ryu, S.-O.; Hwang, S. M.; Rabinowitz, M. J. Shock tube and modeling study of the H + O_2 = OH + O reaction over a wide range of composition, pressure, and temperature. *J. Phys. Chem.* **1995**, *99*, 13984−13991.

(13) Melius, C. F.; Blint, R. J. The potential energy surface of the HO_2 molecular system. *Chem. Phys. Lett.* **1979**, *64*, 183−189.

(14) Varandas, A. J. C.; Brandao, J. A double many-body expansion of molecular potential energy functions II. Application to selected AB_2

van der Waals molecules and more stable molecules: the ground state surfaces of HeH_2, $HeLi_2$, and HO_2. *Mol. Phys.* **1986**, *57*, 387.
(15) Varandas, A. J. C.; Brandao, J.; Quintales, L. A. M. A realistic HO_2 potential energy surface from the double many-body expansion method. *J. Phys. Chem.* **1988**, *92*, 3732−3742.
(16) Pastrana, M. R.; Quintales, L. A. M.; Brandao, J.; Varandas, A. J. C. Recallibration of a single-valued double many body expansion potential energy surface for ground state HO_2 and dynamics calculations for the O+OH → O_2+H reaction. *J. Phys. Chem.* **1990**, *94*, 8073−8088.
(17) Kendrick, B.; Pack, R. T. Potential energy surfaces for the low-lying 2A″ and 2A′ states of HO_2: use of the diatomics in molecules model to fit ab initio data. *J. Chem. Phys.* **1995**, *102*, 1994−2012.
(18) Xu, C.; Xie, D.; Zhang, D. H.; Lin, S. Y.; Guo, H. A new ab initio potential energy surface of $HO_2(X^2A')$ and quantum studies of HO_2 vibrational spectrum and rate constants for the H + O_2 ↔ O + OH reactions. *J. Chem. Phys.* **2005**, *122*, 244305.
(19) Xie, D.; Xu, C.; Ho, T.-S.; Rabitz, H.; Lendvay, G.; Lin, S. Y.; Guo, H. Global analytical potential energy surfaces for $HO_2(X^2A'')$ based on high level ab initio calculations. *J. Chem. Phys.* **2007**, *126*, 074315.
(20) Varandas, A. J. C. Accurate combined-hyperbolic-inverse-power-representation of ab initio potential energy surface for the hydroperoxyl radical and dynamics study of O+OH reaction. *J. Chem. Phys.* **2013**, *138*, 134117.
(21) Li, A.; Xie, D.; Dawes, R.; Jasper, A. W.; Ma, J.; Guo, H. Global potential energy surface, vibrational spectrum, and reaction dynamics of the first excited A^2A' state of HO_2. *J. Chem. Phys.* **2010**, *133*, 144306.
(22) Lin, S. Y.; Xie, D.; Guo, H. Revelation of non-statistical behavior in HO_2 vibration by a new ab initio potential energy surface. *J. Chem. Phys.* **2006**, *125*, 091103.
(23) Lin, S. Y.; Rackham, E. J.; Guo, H. Quantum mechanical rate constants for H + O_2 ↔ O + OH and H + O_2 → HO_2 reactions. *J. Phys. Chem. A* **2006**, *110*, 1534−1540.
(24) Lin, S. Y.; Guo, H.; Honvault, P.; Xie, D. Quantum dynamics of the H + O_2 → O + OH reaction on an accurate ab initio potential energy surface. *J. Phys. Chem. B* **2006**, *110*, 23641−23643.
(25) Honvault, P.; Lin, S. Y.; Xie, D.; Guo, H. Differential and integral cross sections for the H + O_2 → OH + O combustion reaction. *J. Phys. Chem. A* **2007**, *111*, 5349−5352.
(26) Xu, C.; Jiang, B.; Xie, D.; Farantos, S. C.; Lin, S. Y.; Guo, H. Analysis of the HO_2 vibrational spectrum on an accurate ab initio potential energy surface. *J. Phys. Chem. A* **2007**, *111*, 10353−10361.
(27) Hankel, M.; Smith, S. C.; Meijer, A. J. H. M. State-to-state reaction probabilities for the H + O_2(v,j) → O + OH(v′,j′) reaction on three potential energy surfaces. *J. Chem. Phys.* **2007**, *127*, 064316.
(28) Lin, S. Y.; Guo, H.; Honvault, P.; Xu, C.; Xie, D. Accurate quantum mechanical calculations of differential and integral cross sections and rate constant for the O + OH reaction using an ab initio potential energy surface. *J. Chem. Phys.* **2008**, *128*, 014303.
(29) Lin, S. Y.; Sun, Z.; Guo, H.; Zhang, D. H.; Honvault, P.; Xie, D.; Lee, S.-Y. Fully Coriolis coupled quantum studies of the H + O_2 → OH + O reaction on an accurate potential energy surface: integral cross sections and rate constants. *J. Phys. Chem. A* **2008**, *112*, 602−611.
(30) Sun, Z.; Zhang, D. H.; Xu, C.; Zhou, S.; Xie, D.; Lendvay, G.; Lee, S.-Y.; Lin, S. Y.; Guo, H. State-to-state dynamics of H + O_2 reaction. Evidence for nonstatistical behavior. *J. Am. Chem. Soc.* **2008**, *130*, 14962−14963.
(31) Quéméner, G.; Balakrishnan, N.; Kendrick, B. K. Quantum dynamics of the O+OH→H+O_2 reaction at low temperatures. *J. Chem. Phys.* **2008**, *129*, 224309.
(32) Lique, F.; Jorfi, M.; Honvault, P.; Halvick, P.; Lin, S. Y.; Guo, H.; Xie, D. Q.; Dagdigian, P. J.; Kłos, J.; Alexander, M. H. O+OH → O_2+H: A key reaction for interstellar chemistry. New theoretical results and comparison with experiment. *J. Chem. Phys.* **2009**, *131*, 221104.
(33) Ma, J.; Lin, S. Y.; Guo, H.; Sun, Z.; Zhang, D. H.; Xie, D. State-to-state quantum dynamics of the O + OH → H + O_2 reaction. *J. Chem. Phys.* **2010**, *133*, 054302.
(34) Juanes-Marcos, J. C.; Quéméner, G.; Kendrick, B. K.; Balakrishnan, N. Ultracold collisions and reactions of vibrationally excited OH radicals with oxygen atoms. *Phys. Chem. Chem. Phys.* **2011**, *13*, 19067−19076.
(35) Perry, J. W.; Dawes, R.; Wagner, A. F.; Thompson, D. L. A classical trajectory study of the intramolecular dynamics, isomerization, and unimolecular dissociation of HO_2. *J. Chem. Phys.* **2013**, *139*, 084319.
(36) Walch, S. P.; Duchovic, R. J. Theoretical characterization of the potential energy surface for H+O_2 = HO*$_2$ = OH+O. III. Computed points to define a global potential energy surface. *J. Chem. Phys.* **1991**, *94*, 7068−7075.
(37) Yarkony, D. R. Diabolical conical intersections. *Rev. Mod. Phys.* **1996**, *68*, 985−1013.
(38) Domcke, W.; Yarkony, D. R. Role of conical intersections in molecular spectroscopy and photoinduced chemical dynamics. *Annu. Rev. Phys. Chem.* **2012**, *63*, 325−352.
(39) Kendrick, B. K.; Hazra, J.; Balakrishnan, N. The geometric phase controls ultracold chemistry. *Nat. Commun.* **2015**, *6*, 7918.
(40) Hazra, J.; Kendrick, B. K.; Balakrishnan, N. Importance of geometric phase effects in ultracold chemistry. *J. Phys. Chem. A* **2015**, *119*, 12291−12303.
(41) Huang, J.; Kendrick, B. K.; Zhang, D. H. Mechanistic insights into ultracold chemical reactions under the control of the geometric phase. *J. Phys. Chem. Lett.* **2021**, *12*, 2160−2165.
(42) Longuet-Higgins, H. C.; Öpik, U.; Pryce, M. H. L.; Sack, R. A. Studies of the Jahn-Teller effect. II. The dynamical problem. *Proc. Royal Soc. A (London)* **1958**, *244*, 1−16.
(43) Berry, M. V. Quantal phase factors accompanying adiabatic changes. *Proc. Royal Soc. A (London)* **1984**, *392*, 45−57.
(44) Mead, C. A. The geometric phase in molecular systems. *Rev. Mod. Phys.* **1992**, *64*, 51−85.
(45) Baer, M. *Beyond Born-Oppenheimer: Electronic Nonadiabatic Coupling Terms and Conical Intersections*; Wiley: Hoboken, 2006.
(46) Yarkony, D. R. Nonadiabatic quantum chemistry - past, present and future. *Chem. Rev.* **2012**, *112*, 481−498.
(47) Ryabinkin, I. G.; Joubert-Doriol, L.; Izmaylov, A. F. Geometric phase effects in nonadiabatic dynamics near conical intersections. *Acc. Chem. Res.* **2017**, *50*, 1785−1793.
(48) Xie, C.; Malbon, C. L.; Guo, H.; Yarkony, D. R. Up to a sign. The insidious effects of energetically inaccessible conical intersections on unimolecular reactions. *Acc. Chem. Res.* **2019**, *52*, 501−509.
(49) Meek, G. A.; Levine, B. G. Wave function continuity and the diagonal Born-Oppenheimer correction at conical intersections. *J. Chem. Phys.* **2016**, *144*, 184109.
(50) Xie, C.; Yarkony, D. R.; Guo, H. Nonadiabatic tunneling via conical intersections and the role of the geometric phase. *Phys. Rev. A* **2017**, *95*, 022104.
(51) Köppel, H. Diabatic representation methods for the construction of diabatic electronic states. In *Conical Intersections: Electronic Structure, Dynamics and Spectroscopy*; Domcke, W., Yarkony, D. R., Köppel, H., Eds.; World Scientific, 2004.
(52) Guo, H.; Yarkony, D. R. Accurate nonadiabatic dynamics. *Phys. Chem. Chem. Phys.* **2016**, *18*, 26335−26352.
(53) Knowles, P. J.; Werner, H.-J. An efficient method for the evaluation of coupling coefficients in configuration interaction calculations. *Chem. Phys. Lett.* **1988**, *145*, 514−522.
(54) Werner, H.-J.; Knowles, P. J. An efficient internally contracted multiconfiguration−reference configuration interaction method. *J. Chem. Phys.* **1988**, *89*, 5803−5814.
(55) Davidson, E. R.; Silver, D. W. Size consistency in the dilute helium gas electronic structure. *Chem. Phys. Lett.* **1977**, *52*, 403−406.
(56) Dunning, T. H. Gaussian basis sets for use in correlated molecular calculations. I. The atoms boron through neon and hydrogen. *J. Chem. Phys.* **1989**, *90*, 1007−1023.

https://doi.org/10.1021/acs.jctc.3c00291
J. Chem. Theory Comput. 2023, 19, 2929−2938

(57) Knowles, P. J.; Werner, H.-J. An efficient second-order MC SCF method for long configuration expansions. *Chem. Phys. Lett.* **1985**, *115*, 259−267.
(58) Werner, H.-J.; Knowles, P. J. A second order multiconfiguration SCF procedure with optimum convergence. *J. Chem. Phys.* **1985**, *82*, 5053−5063.
(59) Werner, H. J.; Knowles, P. J.; Knizia, G.; Manby, F. R.; Schütz, M. Molpro: a general-purpose quantum chemistry program package. *WIREs Comput. Mol. Sci.* **2012**, *2*, 242−253.
(60) Mead, C. A.; Truhlar, D. G. Conditions for the definition of a strictly diabatic electronic basis for molecular systems. *J. Chem. Phys.* **1982**, *77*, 6090−6098.
(61) Baer, M. Adiabatic and diabatic representations for atom-molecule collisions: Treatment of the collinear arrangement. *Chem. Phys. Lett.* **1975**, *35*, 112−118.
(62) Subotnik, J. E.; Alguire, E. C.; Ou, Q.; Landry, B. R.; Fatehi, S. The requisite electronic structure theory to describe photoexcited nonadiabatic dynamics: Nonadiabatic derivative couplings and diabatic electronic couplings. *Acc. Chem. Res.* **2015**, *48*, 1340−1350.
(63) Dobbyn, A. J.; Knowles, P. J. A comparative study of methods for describing non-adiabatic coupling: diagomic representation of the $^1\Sigma^+/^1\Pi$ HOH and HHO conical intersections. *Mol. Phys.* **1997**, *91*, 1107−1123.
(64) van Harrevelt, R.; van Hemert, M. C. Photodissociation of water. I. Electronic structure calculations for the excited states. *J. Chem. Phys.* **2000**, *112*, 5777−5786.
(65) Jiang, B.; Xie, D.; Guo, H. Communication: State-to-state differential cross sections for $H_2O(B)$ photodissociation. *J. Chem. Phys.* **2011**, *134*, 231103.
(66) Simah, D.; Hartke, B.; Werner, H.-J. Photodissociation dynamics of H_2S on new coupled ab initio potential energy surfaces. *J. Chem. Phys.* **1999**, *111*, 4523−4534.
(67) Kurkal, V.; Fleurat-Lessard, P.; Schinke, R. NO_2: Global potential energy surfaces of the ground ($1\,^2A_1$) and the first excited ($1\,^2B_2$) electronic states. *J. Chem. Phys.* **2003**, *119*, 1489−1501.
(68) Xie, C.; Hu, X.; Zhou, L.; Xie, D.; Guo, H. Ab initio determination of potential energy surfaces for the first two UV absorption bands of SO_2. *J. Chem. Phys.* **2013**, *139*, 014305.
(69) Yarkony, D. R. Conical intersections: Diabolical and often misunderstood. *Acc. Chem. Res.* **1998**, *31*, 511−518.
(70) Yarkony, D. R. Energies and derivative couplings in the vicinity of a conical intersection using degenerate perturbation theory and analytic gradient techniques. 1. *J. Phys. Chem. A* **1997**, *101*, 4263−4270.
(71) Malbon, C. L.; Zhu, X.; Guo, H.; Yarkony, D. R. On the incorporation of the geometric phase in general single potential energy surface dynamics: A removable approximation to ab initio data. *J. Chem. Phys.* **2016**, *145*, 234111.
(72) Xie, C.; Zhu, X.; Yarkony, D. R.; Guo, H. Permutation invariant polynomial neural network approach to fitting potential energy surfaces. IV. Coupled diabatic potential energy matrices. *J. Chem. Phys.* **2018**, *149*, 144107.
(73) Braams, B. J.; Bowman, J. M. Permutationally invariant potential energy surfaces in high dimensionality. *Int. Rev. Phys. Chem.* **2009**, *28*, 577−606.
(74) Jiang, B.; Guo, H. Permutation invariant polynomial neural network approach to fitting potential energy surfaces. *J. Chem. Phys.* **2013**, *139*, 054112.
(75) Li, J.; Jiang, B.; Guo, H. Permutation invariant polynomial neural network approach to fitting potential energy surfaces. II. Four-atom systems. *J. Chem. Phys.* **2013**, *139*, 204103.
(76) Malbon, C. L.; Zhao, B.; Guo, H.; Yarkony, D. R. On the nonadiabatic collisional quenching of OH(A) by H_2: a four coupled quasi-diabatic state description. *Phys. Chem. Chem. Phys.* **2020**, *22*, 13516−13527.
(77) Guan, Y.; Guo, H.; Yarkony, D. R. Neural network based quasi-diabatic Hamiltonians with symmetry adaptation and a correct description of conical intersections. *J. Chem. Phys.* **2019**, *150*, 214101.
(78) Guan, Y.; Guo, H.; Yarkony, D. R. Extending the representation of multistate coupled potential energy surfaces to include properties operators using neural networks: Application to the $1,2^1A$ states of ammonia. *J. Chem. Theory Comput.h* **2020**, *16*, 302−313.
(79) Guan, Y.; Xie, C.; Guo, H.; Yarkony, D. R. Neural network based quasi-diabatic representation for S_0 and S_1 states of formaldehyde. *J. Phys. Chem. A* **2020**, *124*, 10132−10142.
(80) Wang, Y.; Guan, Y.; Guo, H.; Yarkony, D. R. Enabling complete multichannel nonadiabatic dynamics: A global representation of the two-channel coupled, $1,2^1A$ and 1^3A states of NH_3 using neural networks. *J. Chem. Phys.* **2021**, *154*, 094121.
(81) Guan, Y.; Xie, C.; Guo, H.; Yarkony, D. R. Enabling a unified description of both internal conversion and intersystem crossing in formaldehyde: A global coupled quasi-diabatic Hamiltonian for its S_0, S_1, and T_1 states. *J. Chem. Theory Comput.h* **2021**, *17*, 4157−4168.
(82) Jiang, B.; Li, J.; Guo, H. Potential energy surfaces from high fidelity fitting of ab initio points: The permutation invariant polynomial-neural network approach. *Int. Rev. Phys. Chem.* **2016**, *35*, 479−506.
(83) Guan, Y.; Xie, C.; Yarkony, D. R.; Guo, H. High-fidelity first principles nonadiabaticity: Diabatization, analytic representation of global diabatic potential energy matrices, and quantum dynamics. *Phys. Chem. Chem. Phys.* **2021**, *23*, 24962−24983.
(84) Bunker, P. R.; Jensen, P. *Molecular Symmetry and Spectroscopy*; NRC Research Press: Ottawa, 1998.
(85) Raff, L. M.; Komanduri, R.; Hagan, M.; Bukkapatnam, S. T. S. *Neural Networks in Chemical Reaction Dynamics*; Oxford University Press: Oxford, 2012.
(86) Lubic, K. G.; Amano, T.; Uehara, H.; Kawaguchi, K.; Hirota, E. The ν_1 band of the DO_2 radical by difference frequency laser and diode laser spectroscopy: The equilibrium structure of the hydroperoxyl radical. *J. Chem. Phys.* **1984**, *81*, 4826−4831.
(87) Howard, C. J. Kinetic study of the equilibrium $HO_2 + NO \leftrightarrow OH + NO_2$ and the thermochemistry of HO_2. *J. Am. Chem. Soc.* **1980**, *102*, 6937−6941.
(88) Litorja, M.; Ruscic, B. A photoionization study of the hydroperoxyl radical, HO_2, and hydrogen peroxide, H_2O_2. *J. Electron Spectrosc. Relat. Phenom.* **1998**, *97*, 131−146.
(89) Harding, L. B.; Maergoiz, A. I.; Troe, J.; Ushakov, V. G. Statistical rate theory for the $HO+O \leftrightarrow HO_2 \leftrightarrow H+O_2$ reaction system: SACM/CT calculations between 0 and 5000 K. *J. Chem. Phys.* **2000**, *113*, 11019−11034.
(90) Huber, K. P.; Herzberg, G. *Molecular Spectra and Molecular Structure, IV, Constants of Diatomic Molecules*; Springer, New York, 1979.

https://doi.org/10.1021/acs.jctc.3c00291
J. Chem. Theory Comput. 2023, 19, 2929−2938